IOSR Journal Of Applied Physics (IOSR-JAP)
e-ISSN: 2278-4861.Volume 17, Issue 5 Ser. I (Sept – Oct 2025), PP 01-09
www.Iosrjournals.Org

A Green And Sustainable Approach For The Synthesis Of Cuo, Ceo_2, And Cuo@Ceo_2 Core-Shell Nanomaterials: A Comprehensive Characterization

Kundan Kaur And Narendra Babu Simhachalam
Department Of Physics, Osmania University, Hyderabad-500007, India.

Abstract
Our study presents a facile and eco-friendly sol-gel technique for synthesizing pure copper oxide (CuO), cerium oxide (CeO_2), and CuO@CeO_2 core-shell nanoparticles (CS-NPs), utilizing aloe vera gel (AVG) as a natural capping agent. The photocatalysts' structural, morphological, and optical properties were thoroughly characterized using a suite of analytical techniques, including X-ray photoelectron spectroscopy (XPS), powder-X-ray diffraction (p-XRD), FESEM-EDX, FT-IR, and Raman spectral studies. P-XRD analysis confirmed the successful formation of the core-shell nanostructures.

Date of Submission: 27-08-2025 Date of Acceptance: 07-09-2025

I. Introduction

Green synthesis of metal oxides has gained significant interest over the past few decades, primarily due to their applications in environmental, energy, and biomedical fields. Copper oxide (CuO) nanoparticles, in particular, are highly valued [1]. These nanoparticles, which typically have a monoclinic crystal structure and are a p-type semiconductor, possess unique properties like electron correlation effects, superconductivity, non-toxicity, and stability. Due to these attributes, they've found uses in lithium-ion batteries [2], supercapacitors [3], sensors [4], and are particularly effective in photocatalysis [5,6]. Their ability to adsorb heavy metals and remove organic pollutants also makes them valuable for wastewater treatment.

Cerium oxide (CeO_2) nanoparticles are another class of nanomaterials with remarkable properties such as high oxygen storage capacity, wide band gap, and ability to easily transition between the Ce^{4+} and Ce^{3+} oxidation states. This makes them ideal for heterogeneous photocatalysis. Additionally, their antioxidant and antibacterial properties make them promising for biomedical applications like drug delivery and wound healing [7-9].

The formation of core-shell nanoparticles (CS-NPs) [10] is an area of growing research interest, as these structures often exhibit enhanced properties related to their pure metal oxide NPs. Based on this, our research focuses on a straightforward sol-gel route using AVG as a capping agent to synthesize pure CuO, CeO_2, and CuO@CeO_2 CS-NPs. These materials were systematically characterized to understand their structural, morphological, and optical properties using several methods like XRD, XPS, SEM, EDX, FTIR, and Raman spectroscopy.

II. Experimental Section

Materials

The substances which are used in the preparation method such as copper nitrate trihydrate [$Cu(NO_3)_2$ $3H_2O$], Ceric Ammonium nitrate [$(NH_4$ $Ce(NO_3)_6$], deionized water, ethylene glycol and ammonia, were ~~purchased~~ procured from M/S SRL Pvt. Ltd., India and M/S Sigma-Aldrich, USA and used without further purification. The AVG was used in the synthesis process of the entire nanomaterials under study.

Synthesis of Pure CuO Nanomaterials [12]

Pure CuO NPs were prepared by a simple sol-gel technique. The method involves liquifying 5 g of $Cu(NO_3)_2{\cdot}3H_2O$ in 60 ml of distilled water (DW). Simultaneously, 2.5 g of aloe vera gel was dispersed in 15ml of deionized water. For the formation of homogeneous solution mixing of these two solutions and kept for 15 min on magnetic stirrer. The resultant solution was continuously stirred overnight on a magnetic stirrer. After approximately 24 h, the solution's pH was between 7 - 8 by adding of ammonia. Following the pH adjustment, then heated blend at 75°C for 4h, then dropwise addition of AVG solution, leading to the formation of a gel. This gel was then heated above 150°C, which initiated a combustion reaction. The resulting raw CuO solid mixture

was collected, crushed for 30 min, and subsequently calcinated at 500°C for 3 h. Finally, the calcined solid material was crushed for an additional 20 minutes to obtain the desired fine pristine CuO NPs.

Synthesis of Pure CeO_2 nano materials [12]

Using a simple sol-gel method with AVG, we synthesized pure cerium oxide (CeO_2) nanoparticles. The process involved dissolving 5g of ceric ammonium nitrate (CAN) in 60 ml of purified water, while simultaneously mixing 2.5g of aloe vera gel with 20 ml of DW. Then, for the formation of a homogeneous mixture above two solutions were slowly combined and stirred for 15 min. After being constant stirred overnight, the pH was adjusted to 7 - 8 by adding ammonia, followed by heating at 70°C and the dropwise addition of ethylene glycol, which resulted in a gel-like substance. This gel was heated above 160°C to initiate a combustion reaction, yielding a powder that was then ground and calcinated at 500°C for 3 h, ultimately producing the free flow solid NPs of pristine CeO_2.

Preparation of CS-based CuO@CeO_2 NPs [12]

We successfully synthesized CuO@CeO_2 CS-NPs via a straightforward sol-gel method using AVG. The process began by preparing three separate solutions: one with 5 g of $Cu(NO_3)_2{\cdot}3H_2O$ in 60ml of DW (sol-1), a second with 11.345 g of $(NH4)_2Ce(NO_3)_6$ also in DW (sol-2), and a third with 3 g of AVG. The AVG solution was first added to the sol-1, followed by the addition of the sol-2 to create a single miscible solution, which was then stirred continuously 24h. After neutralizing the solution with ammonia, it was heated at 60°C, and excess AVG solution was added dropwise, leading to the formation of a gel. This gel was subsequently heated at 250°C, where a combustion reaction produced a powder. The powder was then ground and calcinated at 500°C for 3h, followed by further grinding to get the final fine CuO@CeO_2 CS-NPs.

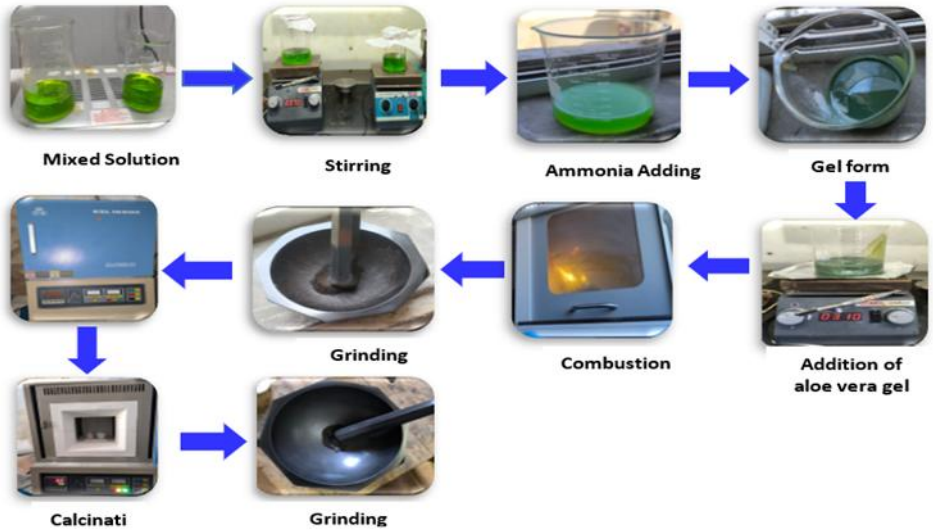

Figure 1. A Graphical representation of green approach for preparation pure and CS-NPs.

III. Results And Discussion

X-Ray diffraction spectroscopy

Figure 2 displays p-XRD patterns of the synthesized nanoparticles. The XRD patterns for the pure CuO, pure CeO_2, and CuO@CeO_2 CS-NPs confirm their crystalline nature and phase purity.

The pink pattern corresponds to the pure CuO nanoparticles. All major diffraction peaks are clearly visible and match the standard monoclinic crystal structure of CuO (JCPDS card No. 48-1548) [11]. The sharp peaks at 2θ values of approximately 35.5°, 38.7°, 48.7°, and 61.5° can be indexed to the (-111), (111), (-202), and (-113) crystal planes, respectively. These sharp and exact peaks indicate that the synthesized CuO NPs are extremely crystalline with a well-formed structure.

The red pattern represents the pure CeO_2 nanoparticles. The observed peaks are in–coincide with the typical cubic fluorite crystal system of CeO_2 (JCPDS card No. 43-1002) [13]. The representative peaks at approximately 56.3°, 47.5°, 33.1°, and 28.5° indexed with the (311), (220), (200), and (111) crystal planes, respectively. The distinct and intense peaks confirm the fruitful preparation of extremely crystalline pristine CeO_2 NPs. The dominance of the (111) peak suggests a preferred growth orientation along this plane.

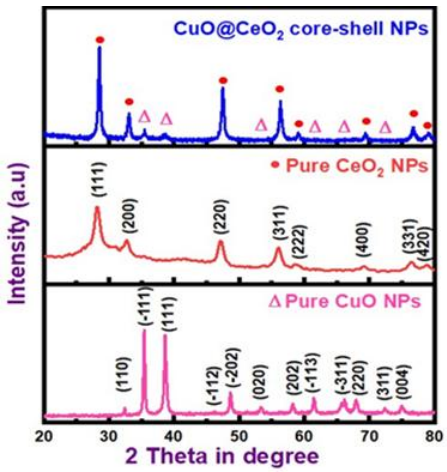

Figure 2. p-XRD spectra of pristine CuO, CeO_2 NPs, and CuO@CeO_2 CS-NPs.

The blue pattern shows the p-XRD pattern of the CuO@CeO_2 CS-NPs. This pattern is particularly significant as it features diffraction peaks from both the CuO core and the CeO_2 shell. The peaks corresponding to the monoclinic CuO phase (Δ) and the cubic fluorite CeO_2 phase (•) are all present, confirming the fruitful fabrication of the CS nanostructure. The presence of peaks from both phases without any new peaks or impurity phases designates the highly pure of the prepared nanocomposite. The intensity and sharpness of the peaks from both materials suggest that the core and shell components maintain their distinct crystalline structures, with no significant interaction causing phase transformation. This coexistence of both sets of peaks is a critical piece of indication for the successful fabrication of the CS-heterostructure. The broadness of the peaks, when compared to the pure materials, may also provide insights into the smaller crystallite size or a change in the lattice strain within the core-shell structure.

Furthermore, the XRD analysis of CuO@CeO_2 core-shell NPs revealed the existence of diffraction peaks related to monoclinic CuO (marked as **Δ**) and cubic fluorite CeO_2 (marked as ●) crystal structures.

In addition, the size of crystalline particles of pristine CuO, CeO_2 NPs, and CuO@CeO_2 CS-NPs were computed from Debye-Scherrer's equation (**$D= K\lambda /\beta \cos\theta$**) which are found to be 40.491 nm, 12.017 nm, and 59.379 nm respectively.

X-Ray photoelectron spectroscopy

To study chemical states and elemental compositions of the synthesized pure CuO, pure CeO_2, and CuO@CeO_2 CS-NPs, XPS was performed. The obtained XPS spectra are represented in Figures 3a to 3c. The analysis consists of Cu (2p), Ce (3d), O (1s), and C (1s) spectra.

The XPS spectra confirm the chemical state and surface composition of the synthesized CuO nanoparticles [14,15]. The Cu 2p spectrum (top right panel) shows two main spin-orbit split peaks at Cu ($2p_{1/2}$) at 954.8 and Cu ($2p_{3/2}$) at 934.8 eV. These peaks, along with the characteristic sat. peaks at 943.5 and 962.0 eV, are definitive indicators of the Cu^{2+} oxidation state, which is characteristic of CuO. The presence of these prominent satellite features is a key signature that distinguishes Cu^{2+} from the Cu^{+} state of Cu_2O, which lacks these satellites.

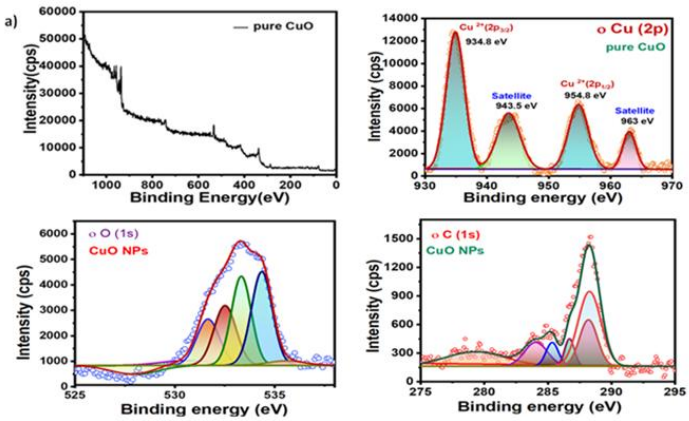

Figure 3a XPS pattern of pristine CuO NPs.

The O 1s spectrum (bottom left panel) is deconvoluted into multiple components, indicating various oxygen species on the surface. The main peak at approximately 529.6 eV matches the lattice oxygen in the CuO crystal lattice. The second peak at a high binding energy (BE) value at 531.6 eV can be assigned to surface hydroxyl groups ($^{-}$OH) or oxygen vacancies [16]. The C 1s spectrum (bottom right panel) shows a dominant peak at ~284.8 eV, which is commonly assigned to adventitious carbon. This peak originates from carbon contamination from the measurement environment or from residual organic species from the AVG utilized during the synthesis. The presence of this peak is expected and does not impact the analysis of the CuO core material.

The XPS study of the pristine CeO_2 nanoparticles reveals their surface chemistry, confirming the presence of both Ce^{4+} and Ce^{3+} oxidation states, which is a key characteristic of ceria's catalytic and electronic properties.

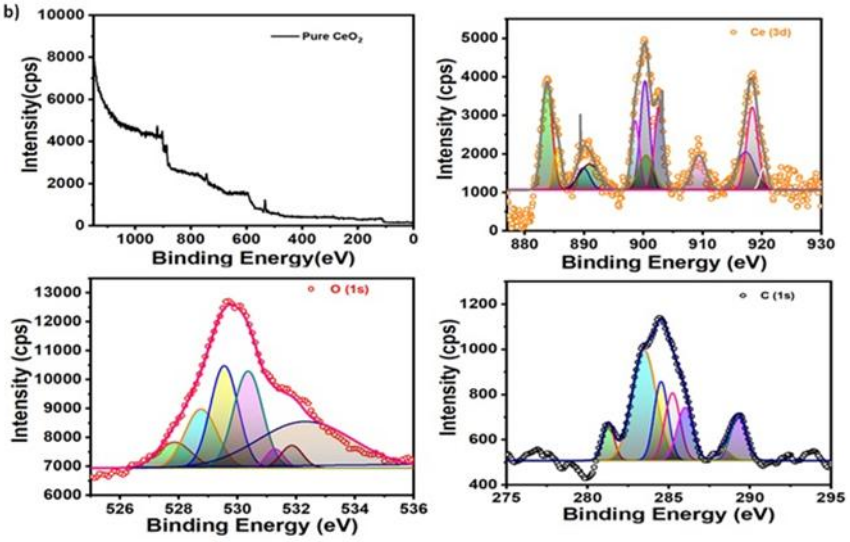

Figure 3b XPS pattern of pristine CeO2 NPs.

The Ce 3d core-level spectrum is particularly complex and rich in information. It consists of multiple spin-orbit split doublets due to final-state effects. This spectrum can be deconvoluted into two main groups of peaks that belong to the Ce^{4+} and Ce^{3+} oxidation states. The peaks centred at 883.6 eV, 885.7 eV, 890.3 eV, 891.2 eV, 898.5 eV are attributed to $3d_{5/2}$ state and the peaks positioned at 900.3 eV, 902.4 eV, 909.4 eV, 917.1 eV, 918.3 eV and 920.5 eV correspond to the $3d_{3/2}$ state. The peaks labelled as v″, v‴ and u″, u‴ belong to Ce^{4+} while peaks v′, v^{o} and u′, u^{o} correspond to the Ce^{3+} state. The coexistence of these two oxidation states is crucial for ceria's function, as the facile interconversion between Ce^{4+} and Ce^{3+} is responsible for its high oxygen storage capacity and redox activity [17]. The presence of Ce^{3+} ions also suggests the formation of oxygen vacancies, which are vital for enhancing photocatalytic activity.

The O 1s core-level spectrum (bottom right panel) is typically deconvoluted into two main peaks. The primary peak at a lesser BE at 529.1 eV is attributed to the lattice held oxygen (O^{2-}) within the ceria lattice. The second peak at a higher BE 531.4 eV is ascribed to surface hydroxyl groups ($^{-}$OH), indicating the surface-active nature of the nanoparticles [18]. The relative proportion of these two peaks can provide information consists of oxygen vacancies on the surface, which are often associated with the occurrence of Ce (III) ions. As with the previous sample, the C 1s spectrum (bottom left panel) shows a dominant peak at 284.7 eV, which is frequently taken as a standard for charge correction and is ascribed to adventitious C (1s) from the sample handling or atmospheric exposure.

The XPS investigation of the $CuO@CeO_2$ CS-NPs confirms the successful formation of the heterostructure by revealing the presence and oxidation states of copper, cerium, and oxygen. The Cu 2p spectrum displays two well-defined peaks at 954.2 (Cu $2p_{1/2}$), and 934.3 eV (Cu $2p_{3/2}$) separated by a spin-orbit splitting of 19.9 eV. This characteristic binding energy difference, along with the existence of shake-up satellite peaks, definitively evidences the presence of the Cu (II) oxidation state, indicating the successful formation of the CuO core.

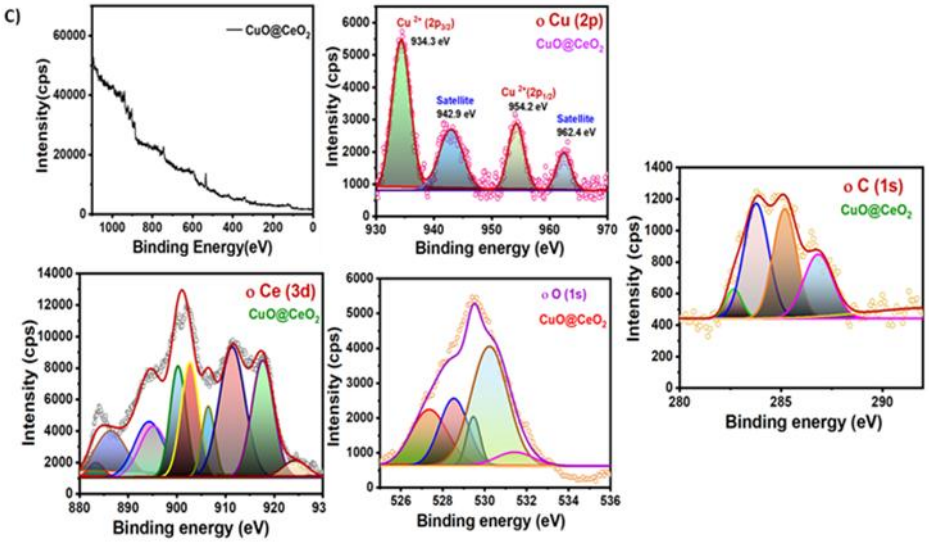

Figure 3c XPS pattern of CuO@CeO2 CS-NPs.

The Ce 3d spectrum is equally informative, showing a complex set of peaks ranging from 883.3 eV to 924.3 eV. The peaks between 883.3 eV and 895.1 eV are designated as $3d_{5/2}$ state, while those from 900.2 eV to 924.3 eV correspond to the $3d_{3/2}$ state. The specific positions and shapes of these peaks confirm the presence of Ce^{4+}, which is the primary oxidation state for CeO_2, further validating the formation of the ceria shell. The O (1s) spectra afford insight into the different oxygen species existing, with peaks from 527.3 eV to 534.1 eV that are attributed to both lattice oxygen within the crystal structure and hydroxyl groups on the nanoparticle surface. Finally, the ubiquitous existence of a C (1s) peak across all samples is a result of adventitious carbon or residual organic material from the AVG used as a capping agent. These combined results from the XPS analysis afford solid indication for the fabrication of the planned core-CuO and shell-CeO_2 nanostructures and complete data given in Table 1.

Table 1. XPS information of pristine CuO, CeO_2, and CuO@CeO_2 CS-NPs.

Nano Material	Cu (2p) eV	Ce (3d) eV	O (1s) eV	C(1s) eV
Pristine CuO	934.7 ($2p_{3/2}$) 943.5 (sat) 954.8 ($2p_{1/2}$) 963.0 (sat)	--	527.9 530.5 531.6 532.5 533.3 534.3 535.5	279.3 284.05 285.3 286.7 288.1 288.2 290.6
Pure CeO_2	--	883.7 ($3d_{5/2}$) 885.8 890.2 891.2 898.5 900.3 ($3d_{3/2}$) 902.4 901.4 917.1 918.3 920.5	527.8 528.8 529.5 530.4 531.3 531.9 532.4	281.3 283.5 284.7 285.2 286.1 288.3 289.4
CuO@CeO_2	934.3 ($2p_{3/2}$) 942.9 954.2 ($2p_{1/2}$) 962.4	883.3 886.3 894.2 895.1 900.2 902.6 906.4 911.3 924.3	527.3 528.5 529.4 530.2 531.4 534.1	246.3 282.6 283.7 285.1 286.8 292.3

Surface morphology

As shown in Figure 4, the FESEM pictures display the surface syllable structure and particle shape of the prepared materials. All three samples, pure CuO, pure CeO_2, and the CuO@CeO_2 core-shell nanoparticles,

tend to agglomerate, a common characteristic of nanoparticles produced via the sol-gel method. This is due to the high surface energy of the nanoparticles, which causes them to cluster together to minimize their overall energy.

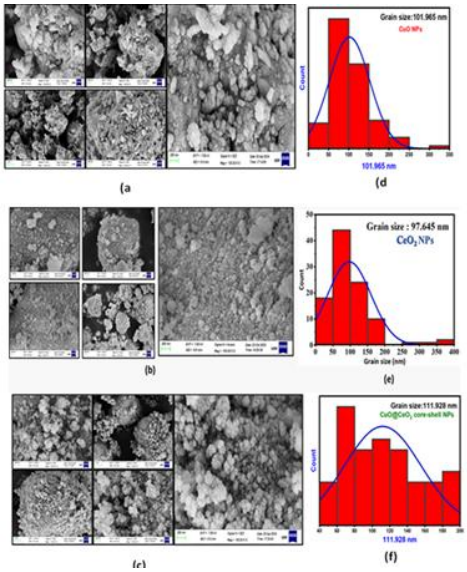

Figure 4 FESEM images of (a) pristine CuO NPs, (b) pristine CeO_2 NPs and (c) CuO@CeO2 CS-NPs; histograms of (d) pristine CuO NPs, (e) pristine CeO_2 NPs and (f) CuO@CeO2 CS-NPs

The morphology of the pure CuO nanoparticles is not entirely uniform. They appear as a mix of quasi-spherical and irregular shapes, which have clustered together to form larger aggregates. Similar to the CuO nanoparticles, the pure CeO2 nanoparticles also show significant agglomeration. The particles are clustered into dense groups, and individual particles are difficult to distinguish clearly. This suggests strong inter-particle forces during synthesis [19]. The core-shell nanoparticles also show agglomeration, consistent with the other samples. However, the overall appearance suggests a distinct change in surface texture, likely due to the formation of the CeO2 shell around the CuO core. This morphology is indicative of a successful core-shell structure where the outer shell modifies the surface properties of the material [20].

The histograms derived from the FESEM images provide a statistical analysis of the grain size distribution for each material, which is a key physical property affecting their performance. The grain size distribution of the pure CuO nanoparticles is centered at 101.96 nm. The histogram is relatively broad, suggesting a variation in particle sizes within the sample. The pure CeO_2 nanoparticles show a mean grain size of 97.145 nm, which is noticeably smaller than that of the pure CuO. The histogram for the core-shell nanoparticles reveals a mean grain size of 111.93 nm. This value is very close to that of the pure CeO_2 nanoparticles. This similarity in size recommends that the overall particle size of the CS-NPs is largely determined by the outer CeO_2 shell. This result further confirms the fruitful fabrication of the core-shell system.

EDX Study

The EDX analysis was achieved to establish the basic composition and purity of the synthesized nanomaterials. The spectra and corresponding elemental tables for each sample, pristine CuO, CeO_2, and the CuO@CeO_2 CS-NPs, are presented in the attached figure. The results provide definitive proof of the elemental composition of each product.

As shown in Figure 5a, the EDAX spectrum for the pure CuO nanoparticles shows strong peaks for Cu and O as the only metallic and non-metallic elements present in significant quantities. The quantitative analysis confirms that the sample is composed of Cu (approximately 79.13 wt% and 50.67 at%) and O (approximately 20.87 wt% and 49.33 at%), which is in close agreement with the theoretical atomic ratio for copper (II) oxide, confirming the extreme pure of the prepared nanomaterial. The absence of other elemental peaks validates that the green synthesis method effectively produced pure CuO nanoparticles without any detectable impurities.

The EDAX spectrum for the pure CeO_2 nanoparticles (Figure 5b) displays distinct peaks corresponding to Ce and O. The quantitative data show that the sample consists of Ce (approximately 83.69 wt% and 38.82 at%) and O (approximately 16.31 wt% and 61.18 at%). This elemental composition confirms the successful formation of pure cerium oxide. The data also support the high purity of the final product, as no other elemental signals were detected.

The EDAX spectrum of the CuO@CeO_2 core-shell nanoparticles (Figure 5c) is particularly important, as it confirms the successful integration of both materials. The spectrum clearly shows the presence of three main

elemental peaks: Cu, Ce, and O. This is conclusive evidence that both copper oxide and cerium oxide are present in the final composite material. The quantitative analysis reveals an elemental composition of Cu (approximately 38.42 wt%), Ce (approximately 32.87 wt%), and O (approximately 28.71 wt%). This finding validates the fabrication of the intended CS system and confirms that the synthesis was successful in producing a composite material containing both CuO and CeO_2. The nonappearance of any other peaks additional attests to the high pure of the final product.

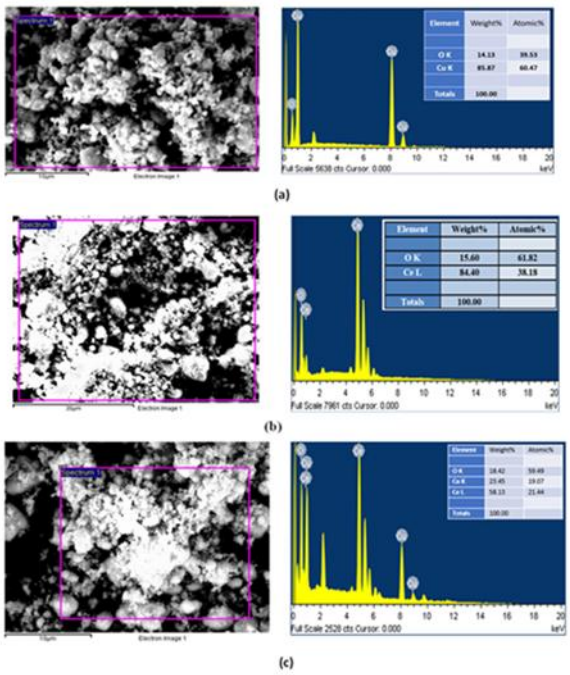

Figure 5. EDAX study of (a) pristine CuO, (b) pristine CeO_2, (c) CuO@CeO_2 CS-NPs.

FTIR spectroscopy

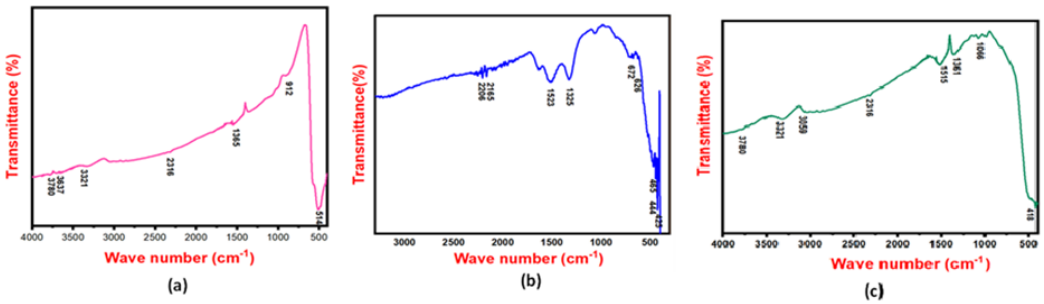

Figure 6. FT-IR Spectrum of (a) pristine CuO, (b) pristine CeO_2, (c) CuO@CeO_2 CS-NPs.

The FT-IR spectra of pristine CuO, CeO_2, and the CuO@CeO_2 CS-NPs were recorded to identify the characteristic vibrational bands and approve the metal oxide bonds present in the prepared materials. The analysis reveals important information about the metal-oxygen bonds and surface-adsorbed groups.

The FTIR spectrum of the pure CuO nanoparticles (Figure 6a) shows a series of prominent peaks. The strong peak in the fingerprint region at 515 cm^{-1} is characteristic of the stretching mode of the Cu-O bond 912 cm^{-1} belongs to the surface hydroxyl groups, corroborating the establishment of CuO. The wide peak at around 3427 cm^{-1} is ascribed to the O-H stretching mode of surface adsorbed water particles or surface -OH groups on the NPs. The small peaks at 1385 cm^{-1} and 1621 cm^{-1} can be related to the bending modes of adsorbed water and the C=O stretching of remaining organic compounds from the AVG used in the synthesis [21].

The FTIR spectrum for the pure CeO_2 nanoparticles (Figure 6b) displays a solid absorption peak at 672 cm^{-1} [22]. This peak is specifically given to the stretching vibration of the Ce-O bond, which confirms the successful synthesis of cerium oxide. Similar to the CuO sample, a broad peak around 3425 $cm^{-1}$and a sharp peak at 1625 cm^{-1} is visible, indicating the existence of surface-adsorbed water and hydroxyl groups. The minor peaks at 1323 cm^{-1} and 1525 cm^{-1} are likely due to the C-O and C=O stretching of residual organic impurities.

The FTIR spectrum of the $CuO@CeO_2$ core-shell nanoparticles (Figure 6c) is particularly significant as it shows the characteristic peaks of both the CuO core and the CeO_2 shell. A strong peak at 616 cm^{-1} is a key identifier, which is a blend or shift of the individual metal-oxygen stretching vibrations from both CuO and CeO_2 . This peak's position confirms the existence of both Cu-O and Ce-O bonds, provided that strong indication for the fabrication of the CS-heterostructure. The broad band around 3316 cm^{-1} and the peak at 1646 cm^{-1} are again given to the O-H stretching and bending modes of adsorbed water, respectively. The peak at 1404 cm^{-1} is also ascribed to the residual organic material. The shift of the metal-oxygen peaks in the CS nanomaterial compared to the pristine compounds indicates a successful interaction between the two components at the interface.

Raman Spectroscopy

To further examine about the chemical structure, crystallinity, and vibrational modes of prepared nano composite, Raman spectroscopy was employed Figure 7 displays Raman spectra of (a) pristine CuO NPs, (b) pristine CeO_2, (c) $CuO@CeO_2$ CS-NPs.

The Raman spectrum for pure CuO (Figure 7a) is consistent with the monoclinic crystal system of CuO. According to group theory, the monoclinic CuO structure has 3 modes are Raman active (A_g+2B_g). The spectrum clearly shows these distinct Raman peaks. The most prominent peak at 276 cm^{-1} is given to the Ag mode. The peaks at 331cm^{-1} and 620 cm^{-1} corresponds to the B_g modes. The other minor peaks at higher wavenumbers are likely from multi-phonon processes [12]. The existence of these typical peaks confirms the successful synthesis of highly crystalline pure CuO nanoparticles.

The Raman spectrum for pure CeO_2 (Figure 7b) is dominated by a single, sharp, and intense peak at 462 cm^{-1}. This peak is the signature Raman-active mode (F_{2g}) of the cubic fluorite structure of CeO_2. The sharpness of this peak indicates a high degree of crystallinity and structural order within the CeO_2 lattice. This is a very reliable fingerprint for pure cerium oxide. The position of this peak is slightly shifted from the bulk value, which can be attributed to the quantum confinement effect in nanocrystalline materials. The minor peak at 610 cm^{-1} is often associated with the presence of defects or oxygen vacancies [23], a crucial feature for ceria's catalytic properties.

The Raman spectrum of the $CuO@CeO_2$ core-shell nanoparticles (Figure 7c) is a composite of the spectra of its individual components. The spectrum shows a mixture of peaks corresponding to both the CuO core and the CeO_2 shell. A strong peak is visible at 447 cm^{-1}, which is a slight downshift from the pure CeO_2 peak at 462 cm^{-1}. This shift is a key piece of evidence for the interfacial interaction between the CuO core and the CeO_2 shell, suggesting a change in the lattice vibrations due to strain or coupling at the heterojunction. Additionally, the characteristic peaks of CuO, particularly the one at 272 cm^{-1} (shifted from the pure CuO peak at 276 cm^{-1}), are also present. The coexistence and slight shifts of these characteristic peaks from both materials in a single spectrum provide compelling suggestion for the fruitful fabrication of the envisioned CS-heterostructure.

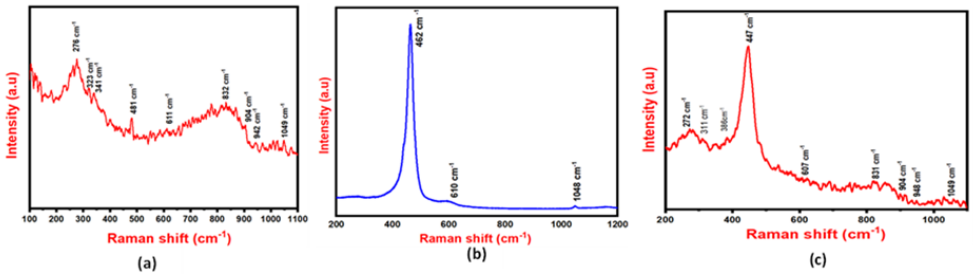

Figure 7. Raman Spectrum of (a) pristine CuO NPs, (b) pristine CeO_2 NPs, (c) $CuO@CeO_2$ CS-NPs.

IV. Conclusion

This research successfully demonstrates a simple and eco-friendly sol-gel method for synthesizing pure CuO, pure CeO_2, and $CuO@CeO_2$ core-shell nanoparticles. The process utilizes aloe vera gel as a natural and non-toxic reducing agent, aligning with green chemistry principles. The comprehensive characterization of the prepared photocatalysts using advanced spectroscopic techniques, including XRD, XPS, FESEM, EDX, FTIR and Raman spectroscopy confirmed the materials' structural and chemical integrity. Specifically, XRD analysis verified the distinct monoclinic crystalline phase of CuO and the cubic fluorite structure of CeO_2. XPS confirmed the elemental composition and oxidation states of the materials, while the other techniques provided further evidence of the successful synthesis. A key finding was the significantly reduced band gap in the $CuO@CeO_2$ core-shell nanoparticles, making them promising candidates for enhanced photocatalytic applications.

References

[1]. S. Pramila, G. Nagaraju, C. Mallikarjunaswamy, K.C. Latha, S. Chandan, Ramith Ramu, V. Rashmi, & V. Lakshmi Ranganatha. (2020). Green Synthesis Of Bivo4 Nanoparticles By Microwave Method Using Aegle Marmelos Juice As A Fuel: Photocatalytic And Antimicrobial Study. Analytical Chemistry Letters, 10(3), 298–306. Https://Doi.Org/10.1080/22297928.2020.1785935

[2]. Wang, C., Higgins, D., Wang, F., Li, D., Liu, R., Xia, G., Li, N., Li, Xu, H., & Wu, G. (2014). Controlled Synthesis Of Micro/Nanostructured Cuo Anodes For Lithium-Ion Batteries. Nano Energy, 9, 334–344. Https://Doi.Org/10.1016/J.Nanoen.2014.08.009

[3]. Dubal, D. P., Gund, G. S., Lokhande, C. D., & Holze, R. (2013). Cuo Cauliflowers For Supercapacitor Application: Novel Potentiodynamic Deposition. 48(2), 923–928. Https://Doi.Org/10.1016/J.Materresbull.2012.11.081

[4]. Reddy, S., Kumara Swamy, B. E., & Jayadevappa, H. (2012). Cuo Nanoparticle Sensor For The Electrochemical Determination Of Dopamine. Electrochimica Acta, 61, 78–86. Https://Doi.Org/10.1016/J.Electacta.2011.11.091

[5]. 5) Ali Taheri Akerdi, & S. Hajir Bahrami. (2019). Application Of Heterogeneous Nano-Semiconductors For Photocatalytic Advanced Oxidation Of Organic Compounds: A Review. Journal Of Environmental Chemical Engineering, 7(5), 103283–103283. Https://Doi.Org/10.1016/J.Jece.2019.103283

[6]. Ahmed, S. N., & Haider, W. (2018). Heterogeneous Photocatalysis And Its Potential Applications In Water And Wastewater Treatment: A Review. Nanotechnology, 29(34), 342001. Https://Doi.Org/10.1088/1361-6528/Aac6ea

[7]. Ma, L., Ai, X., Jiang, W., Liu, P., Chen, Y., Lu, K., Song, X., & Wu, X. (2022). Zn/Ce Metal-Organic Framework-Derived Zno@Ceo_2 Nano-Heterojunction For Enhanced Photocatalytic Activity. Colloids And Interface Science Communications, 49, 100636–100636. Https://Doi.Org/10.1016/J.Colcom.2022.100636

[8]. Masula, K., Bhongiri, Y., Raghav Rao, G., Vijay Kumar, P., Pola, S., & Basude, M. (2022). Evolution Of Photocatalytic Activity Of Ceo_2–Bi2o3 Composite Material For Wastewater Degradation Under Visible-Light Irradiation. Optical Materials, 126, 112201. Https://Doi.Org/10.1016/J.Optmat.2022.112201

[9]. Avelino Corma, Atienzar, P., Hermenegildo García, & Jean-Yves Chane-Ching. (2004). Hierarchically Mesostructured Doped Ceo_2 With Potential For Solar-Cell Use. Nature Materials, 3(6), 394–397. Https://Doi.Org/10.1038/Nmat1129

[10]. Cathrin Lims, S., Divya, S., & Jose, M. (2023). Design Of Cuo @ Sio_2 Core Shell Nanocomposites And Its Applications To Photocatalytic Degradation Of Rhodamine B Dye. Optical Materials, 144, 114356. Https://Doi.Org/10.1016/J.Optmat.2023.114356

[11]. Siddiqui, H., Parra, M. R., Qureshi, M. S., Malik, M. M., & Haque, F. Z. (2018). Studies Of Structural, Optical, And Electrical Properties Associated With Defects In Sodium-Doped Copper Oxide (Cuo/Na) Nanostructures. Journal Of Materials Science, 53(12), 8826–8843. Https://Doi.Org/10.1007/S10853-018-2179-6

[12]. K. Kaur, R. Gade, R. Mitty, V. S. Puli, S. Pola, N. B. Simhachalam, Green Synthesis Of Aloe Vera Gel-Based Zno@Ceo_2 And Ceo_2@Zno Core−Shell Heterostructures For Highly Efficient Visible Light Photocatalytic Mineralization Of Organic Pollutants And Industrial Wastewater, Surfaces And Interfaces, 72 (2025) 107254, Https://Doi.Org/10.1016/J.Surfin.2025.107254.

[13]. Kumar, E., P. Selvarajan, & Balasubramanian, K. (2010). Preparation And Studies Of Cerium Dioxide(Ceo_2) Nanoparticles By Microwave-Assisted Solution Method. Recent Research In Science And Technology, 2(4), 37–41.

[14]. H.N. Jayasimha, K.G. Chandrappa, P.F. Sanaulla, & V.G. Dileepkumar. (2024). Green Synthesis Of Cuo Nanoparticles: A Promising Material For Photocatalysis And Electrochemical Sensor. Sensors International, 5, 100254–100254. Https://Doi.Org/10.1016/J.Sintl.2023.100254

[15]. Li, Z., Xin, Y., Zhang, Z., Wu, H., & Wang, P. (2015). Rational Design Of Binder-Free Noble Metal/Metal Oxide Arrays With Nanocauliflower Structure For Wide Linear Range Nonenzymatic Glucose Detection. Scientific Reports, 5(1). Https://Doi.Org/10.1038/Srep10617

[16]. Hippolyte Todou Assaouka, Daawe, D. M., Roussin Lontio Fomekong, Issah Njiawouo Nsangou, & Kouotou, P. M. (2022). Inexpensive And Easily Replicable Precipitation Of Cuo Nanoparticles For Low Temperature Carbon Monoxide And Toluene Catalytic Oxidation. Heliyon, 8(9), E10689–E10689. Https://Doi.Org/10.1016/J.Heliyon.2022.E10689

[17]. Mitra Malekkiani, Fatemeh Ravari, Abbas, Mehdi Dadmehr, Heiko Groiss, Hasan Ali Hosseini, & Sharif, R. (2022). Fabrication Of Graphene-Based Tio_2@Ceo_2 And Ceo_2@Tio_2 Core–Shell Heterostructures For Enhanced Photocatalytic Activity And Cytotoxicity. Acs Omega, 7(34), 30601–30621. Https://Doi.Org/10.1021/Acsomega.2c04338

[18]. Jiao, J., Wei, Y., Zhao, Z., Liu, J., Li, J., Duan, A., & Jiang, G. (2014). Photocatalysts Of 3d Ordered Macroporous Tio_2-Supported Ceo_2 Nanolayers: Design, Preparation, And Their Catalytic Performances For The Reduction Of Co_2 With H2o Under Simulated Solar Irradiation. Industrial & Engineering Chemistry Research, 53(44), 17345–17354. Https://Doi.Org/10.1021/Ie503333b

[19]. Saha, H., Ankita Dastider, Ferdous, J., Samiya Rahman Mim, Sovendo Talapatra, Das, U., Jamal, M., & Billah, M. M. (2024). Photocatalytic Performance Of Cuo Nps: An Experimental Approach For Process Parameter Optimization For Rh B Dye. Results In Materials, 24, 100614–100614. Https://Doi.Org/10.1016/J.Rinma.2024.100614

[20]. E, Kumar & Selvarajan, P. & Balasubramanian, Krishnamoorthi. (2010). Preparation And Studies Of Cerium Dioxide (Ceo_2) Nanoparticles By Microwave-Assisted Solution Method. Rec. Res. Sci. Technol.. 2. 37-41.

[21]. Yusuf, M., R.M. Muthukrishnan, Khan, R. I., C. Vedhi, K. Sakthipandi, & Kader, S. M. A. (2023). Green Synthesis Of Copper Oxide Nanoparticles Using Amaranthus Dubius Leaf Extract For Sensor And Photocatalytic Applications. Chemical Physics Impact, 7, 100374–100374. Https://Doi.Org/10.1016/J.Chphi.2023.100374

[22]. Katheresan, V.; Kansedo, J.; Lau, S. Y. Efficiency Of Various Recent Wastewater Dye Removal Methods: A Review. Journal Of Environmental Chemical Engineering 2018, 6 (4), 4676–4697.

[23]. Li, J.-F., Zhang, Y.-J., Ding, S.-Y., Panneerselvam, R., & Tian, Z.-Q. (2017). Core–Shell Nanoparticle-Enhanced Raman Spectroscopy. Chemical Reviews, 117(7), 5002–5069. Https://Doi.Org/10.1021/Acs.Chemrev.6b00596